Title

Addressing the sensitivity of signals from solid/liquid ambient pressure XPS (APXPS) measurement

Journal

The Journal of Chemical Physics, 153(4)

ISSN

0021-9606

Authors

Qian, Jin

Baskin, Artem

Liu, Zhi

et al.

Publication Date

2020-07-28

DOI

10.1063/5.0006242

Peer reviewed

Addressing the Sensitivity of Signals from Solid/Liquid Ambient Pressure XPS (APXPS) Measurement

Jin Qian[1,2,3], Artem Baskin[3], Zhi Liu[4,5], David Prendergast[3]*, Ethan J. Crumlin[1,2]*

[1] Advanced Light Source, Lawrence Berkeley National Laboratory, Berkeley, CA 94720, United States;

[2] Chemical Sciences Division, Lawrence Berkeley National Laboratory, Berkeley, CA 94720, United States;

[3] Molecular Foundry, Lawrence Berkeley National Laboratory, Berkeley, CA 94720, United States;

[4] State Key Laboratory of Functional Materials for Informatics, Shanghai Institute of Microsystem and Information Technology, Chinese Academy of Sciences, Shanghai 200050, China

[5] School of Physical Science and Technology, ShanghaiTech University, Shanghai 201210, China

Abstract

Ambient Pressure XPS has demonstrated its great potential in probing the solid/liquid interface, which is a central piece in electrocatalytic, corrosion, and energy storage systems. Despite ambient pressure XPS's advantage of being a surface sensitive characterization technique, **the ability of differentiating the surface adsorbed species (~Å scale) and bulk electrolyte (~10 nm scale) in the spectrum depends on the delicate balance between bulk solution concentration (C), surface coverage (Θ), bulk liquid layer thickness (L), and inelastic mean free path (λ) as a function of photon energy PE**. By investigating a model system of gold dissolving in bromide solution, the connection between theoretical prediction at the atomic resolution and macroscopic observable spectrum is established.

Introduction

The research interests of physicists, chemists and materials scientists have shifted significantly from the study of bulk properties of materials to the system behaviors at the interfaces. [1] The interactions and exchange of ions and electrons occurring at the solid/liquid interface are ubiquitous scenarios in electrocatalytic systems, e.g., CO_2 reduction [2-4], hydrogen evolution reaction [5-9], oxygen evolution reaction [10-15], oxygen reduction reaction [16, 17], nitrogen fixation [18, 19] etc., corrosion, as well as in energy storage systems, eg. lithium ion battery [20, 21]. In order to expedite the understanding, controlling, and optimizing the design of these systems, it is crucial to capture the electron transfer, ion transfer, breaking and remaking of chemical bonds with the

effect of solvation environment at the interface, ideally through the integration of advanced characterization techniques and theoretical models.

Characterization instrumentations possessing the power of atomic resolution can be divided into two classes: imaging (eg. SEM, TEM, etc.) and spectroscopy (eg. XPS, XAS, IR, etc.). Both classes of techniques have profound history in surface science applications, which are usually conducted at Ultra-High Vacuum (UHV). With the increasing demand for *operando*, *in situ* measurements, which are orders of magnitude higher in pressure than UHV, advanced spectroscopy with state-of-the-art modification [22-25] is continuously bridging the pressure gap and is gaining an upper hand in the research of solid/liquid interface. For example, Ambient Pressure XPS [26, 27] demonstrated its ability in the direct observation of the electrical double layer [28] as well as catalytic mechanism [29], *operando* XAS has been employed to study the molecular scale electrode/electrolyte interface [30], infrared nanospectroscopy enables studies of the molecular structure of graphene/liquid interfaces with nanoscale spatial resolution [31].

Despite the exciting development and improvement of Ambient Pressure XPS in the application of probing solid/liquid, fundamental questions regarding the sensitivity of these measurements to interfacial features have not been well addressed in previous literatures. A special yet central request in understanding the solid/liquid interface is to detect and to differentiate surface species from its bulk counterpart. Achieving this atomic scale sensitivity is challenging, because such surface species are at the scale of ~Å scale and furthermore, their signals are buried underneath a bulk liquid layer at the scale of ~10 nm, as illustrated in **Figure 1.** To answer the questions regarding sensitivity, as well as to demonstrate a procedure of connecting atomic understanding to experimental observables, we chose to look at a typical scenario in electrochemistry and corrosion: Br ion dissolving gold. It is a well-studied system with established understanding [32, 33], therefore the goal here is not to repeat the electrochemical findings, but rather to leverage the past knowledge as an excellent opportunity for us to address sensitivity of this ambient pressure XPS measurement unambiguously. With a special focus on connecting atomic level picture **(Figure 1b)** and experiment (**Figure 2)**, we intend to provide a general framework (***ab-initio* MD -> DFT -> analytical model -> *ab-initio* constructed spectrum**) for solid/liquid system revealing the relationship of realistic experimental conditions (photon energy, concentration, coverage (**Figure 3**) etc.) vs. expected spectrum from *ab-initio* (**Figure 4**), therefore providing insights into the understanding of distinct spectroscopic features. Lastly, we arrived at the conclusion that the ability of differentiating the surface adsorbed species (~Å scale) and bulk electrolyte (~10 nm scale) on spectroscopy depends on the delicate balance (**Figure 5**) between solution concentration (C), surface coverage (Θ), bulk liquid layer thickness (L), and inelastic mean free path (λ) as a function of photon energy PE.

Results and Discussions

Connection of Experimental Setup and Theoretical Model

After dip and pull (schematic see reference [28]), a meniscus liquid layer forms with thickness of L on the electrode in the probing area. X-rays were exposed from the bulk liquid region, where this

liquid region is assumed to contain a homogeneously distributed solution [Br-] ion of concentration C. Another surface adsorbed [Br-] ion with a concentration expressed in terms of coverage Θ has a 0.8 e V binding energy higher than solution [Br-]. A schematic illustration, especially mapping the idea model to atomic-scale description from *ab-initio* is provided in **Figure 1**.

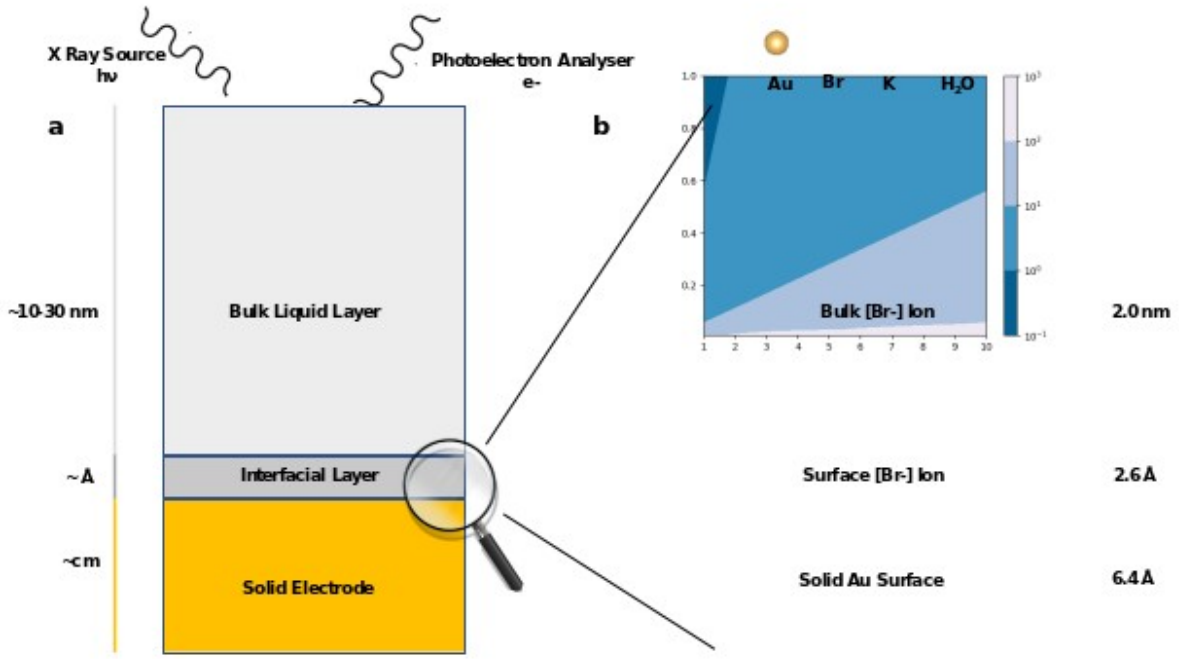

Figure 1. Mapping of the simple schematic model to the atomic scale *ab-initio* model. **a)** Schematic illustration of the homogenous layers model. This model consists of averaged layer of surface species and averaged layer of solution species. X-ray source is from the liquid layer side. The bulk liquid layer thickness is estimated experimentally in reference [28] to be 10-30 nm. Interfacial layer thickness is calculated by taking the average height of surface [Br-] ion in the last 200 equilibrated MD trajectory snapshots. Solid electrode thickness does not contribute to the signal of [Br-] ion. **b)** Atomic scale illustration of the surface species layer and solution species layer, from an equilibrated snapshot of *ab-initio* MD calculation. More frames are provided in Figure 7. Using the *ab-initio* approach, we can calculate the interfacial layer thickness, as well as calculating the BE difference of surface [Br-] ion and solution [Br-] ion, as explained in detail in the parameter space section.

Signals from the X-ray attenuate exponentially according to Beer-Lambert law, $Ix = I_0 * \exp(-x/\lambda)$, where I_0 is the intensity of signal at the depth x = 0, and λ is the inelastic mean free path of the excited photoelectron. The inelastic mean free path of the excited photoelectron generally follows the universal curve, where KE is the kinetic energy of the excited photoelectron, and KE = PE – BE – ϕ. PE is the photon energy of the X-ray beam, BE is the binding energy of the specific element in a specific chemical environment (for example [Br-] in solution and [Br-] on the surface), which could be calculated Quantum Mechanically. ϕ is the work function of the

system of interests, which is cancelled out when calculating the relative binding energy shift. In our experiment, KE is on the range of 4 keV, which gives us λ on the range of 5 nm for metallic system. However, the inelastic mean free path of excited photoelectron in liquid could deviate from that predicted from the universal curve, yielding an approximate λ of 10 nm using tender X-ray, shown in **Table S1** of reference [34], which is calculated using the TPP-2M formulism [35]. A recent study [36] using relativistic full Penn algorithm (FPA) indicated that the IMFPs for liquid water at 4 keV could reach 11 nm.

Surface [Br-] species is assumed to be homogeneously covering the Au surface, with a coverage of Θ monolayer. To summarize, the intensity signals of different species that are made from same element: the intensity of surface [Br-] ion and solution [Br-] ion depends on the combination of L, C, Θ, λ. Given the BE of surface [Br-] ion and solution [Br-] ion, as well as the intensity of signals for surface [Br-] ion and solution [Br-] ion, we can in principle construct the Br 3d spectrum from *ab-initio*, as shown in **Figure 4**.

Description of the Experimental Observations

At 0.6 V vs. Ag/AgCl, dissolution of Au in Br forming $AuBr_4$- in liquid phase is observed through a sharp increase of cyclic voltammetry curve as well as an obvious Br 3d signal at 67 eV to 71 eV. On the contrary, at a negative potential or positive potential less than 0.6 eV, thermodynamic driving force for the dissolution of gold is too small, and no signal of Br 3d is observed due to low concentration of solution [Br-] ion in the liquid phase and low cross-section for Br 3d core-level.

It is interesting to point out that the Br 3d spectrum collected at 0.6 V vs. Ag/AgCl (**Figure 2a** and **Figure 2c**) showed a comparatively symmetrical peak, in contrast of the expected 2:3 (**Figure 2b** and **Figure 2d**) peak feature of 1 M reference $AuBr_4$- solution (4M [Br-] in liquid phase) spectrum due to the spin-orbit splitting of 3d orbital. This change in spectroscopic feature from asymmetric (**Figure 2b**) to symmetric (**Figure 2a**), together with the weakening concave feature (blue arrow in **Figure 2b** and **2d**) at 69.3 eV indicates the possibility of a surface species at a higher binding energy (**Figure 2c**). Given the fact that such surface species' signals of ~Å are buried underneath a bulk liquid layer at the scale of ~10 nm, it is important to address at what conditions such weak signals of surface species can be observable. Furthermore, one should in principle be able to recreate the spectrum (thick black line in **Figure 2c**) *ab-initio* if given the right combinations of the experimental conditions.

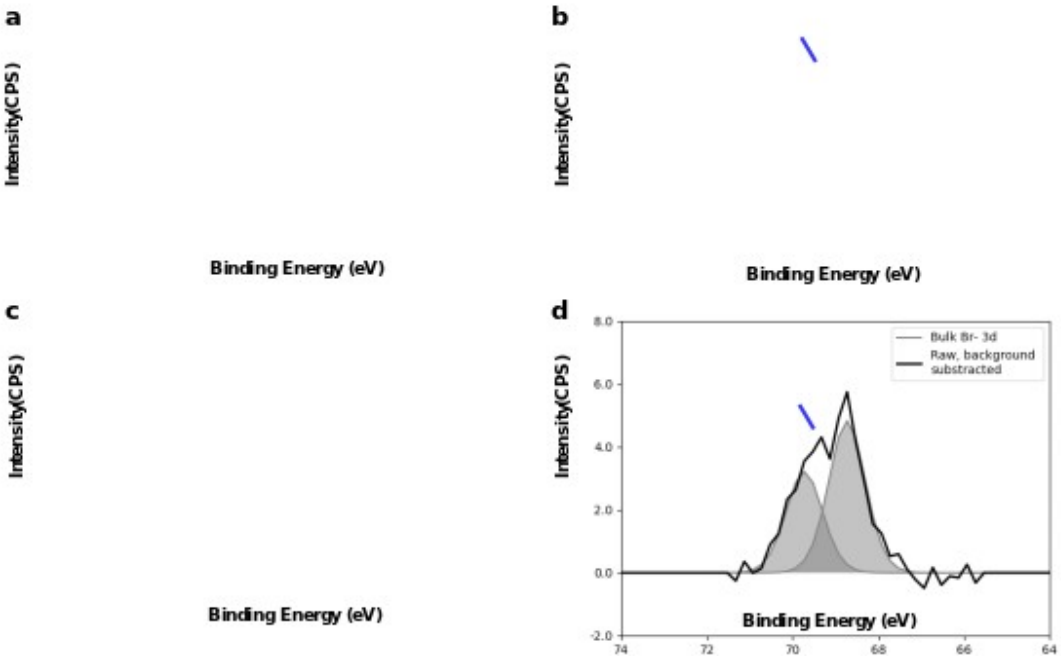

Figure 2. Comparison of Br[3d] spectrum at the condition of 0.6 V vs. Ag/AgCl, and Br 3d spectrum in reference solution of 1M $AuBr_4$-. **a)** Raw spectrum of Br 3d at 0.6 V vs. Ag/AgCl shows a symmetrical feature. **b)** Raw spectrum of Br 3d in reference solution of 1M $AuBr_4$- shows an asymmetrical feature, which has an obvious concave feature at 69.3 eV, indicated by the blue arrow. **c)** Fitted spectrum of Br 3d with background subtracted at 0.6 V vs. Ag/AgCl has an emerging surface species, which contributes to the symmetrical feature. The thick black line is the experimental data with background noise subtracted, and it is what we want to reproduce from *ab-initio*. **d)** Fitted spectrum of Br 3d with subtracted background in reference solution of 1M $AuBr_4$- shows the 2:3 spin-orbit splitting which is 1 eV apart.

Parameter Space

In order to recreate the spectrum, especially the interesting symmetrical featured spectrum of Br 3d at 0.6 V vs. Ag/AgCl, we need to define the lower limit as well as the upper limit of the parameters relevant in **Figure 1**, namely the solution [Br-] ion concentration C, surface [Br-] ion coverage Θ, bulk liquid layer thickness L and the inelastic mean free path λ. We grouped these 4 parameters into chemically relevant one (C and Θ), and measurement relevant one (L and λ). In the following paragraphs, we will describe the upper and lower limit of the parameters with supports from either experiment or theory.

- Layer thickness L is between 10nm to 30 nm in a typical solid/liquid APXPS experimental setup. [28, 37] By assuming that the electrolyte covering the working electrode surface is in the form of a thin layer after the electrochemical treatment, the liquid layer thickness can be obtained from the attenuation of working electrode signal. To show an

extreme version of effect of bulk liquid layer thickness to spectrum, we plotted in **Figure 4a** using a thickness L from 5 nm to 30 nm.

- Inelastic mean free path λ is 11.7nm using the relativistic full Penn algorithm (FPA) at Photon Energy of 4keV. To get more intuition of the effect of inelastic mean free path on the features of spectrum, we chose to vary the mean free path from 5 nm to 15 nm in **Figure 4b**.
- Solution [Br-] ion concentration C is estimated to fall within 2 M to 4 M. It has been observed experimentally that the Br 3d in 1 M KBr solution at 0 V vs. Ag/AgCl didn't show observable intensity, and the Br 3d at 0.6 V vs. Ag/AgCl intensity is not as strong as that in reference 4M solution. The effect of solution [Br-] ion concentration C on spectrum is investigated in **Figure 4c**.
- Surface [Br-] coverage Θ can be derived theoretically from continuum model described in [38], as a function of applied potential and bulk solution concentration, and then be fitted on the Frumkin Isotherm. Here we exploit the experimental guidance and use the "Hurwitz-Parsons" method (Hurwitz, 1965; Dutkiewicz & Parsons, 1966) to construct the adsorption isotherms shown in **Figure 3**. The saturation coverage is on the order of 0.4 monolayer. In order to visualize the effect of surface coverage, we selected a range of surface coverage Θ from 0.1 ML to 0.6 ML and plotted the corresponding *ab-initio* generated spectrum in **Figure 4d**.

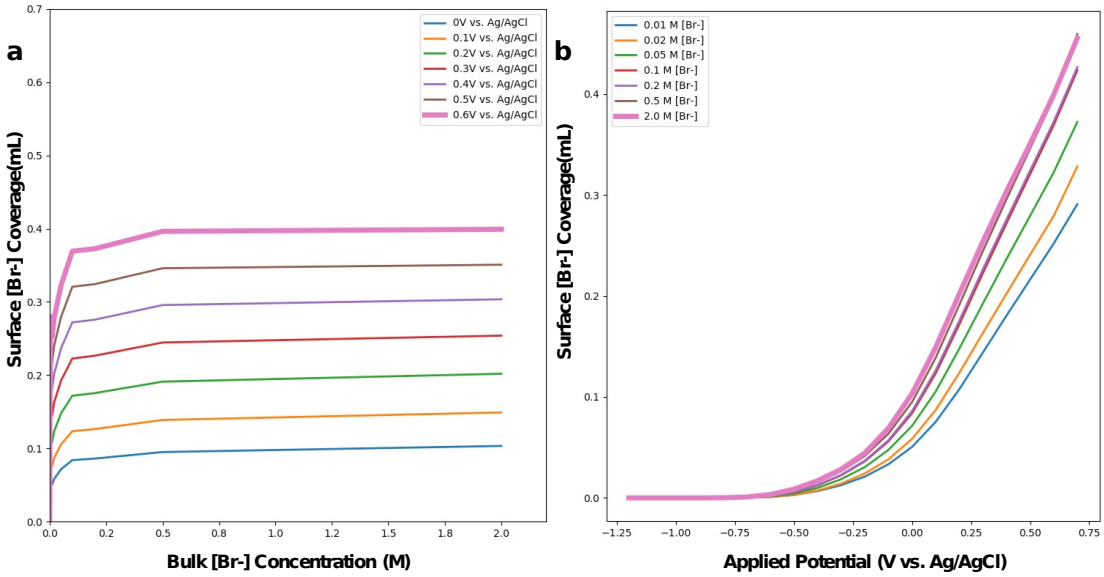

Figure 3. a) Adsorption isotherms at various bulk solution concentration at different potential. Surface [Br-] coverage Θ quickly saturated as bulk solution concentration of [Br-] increases, reaching an equilibrium concentration of 0.4 ML at the realistic condition of 0.6 V vs. Ag/AgCl. **b)** Surface coverage of [Br-] ion in the electrolyte as a function of applied potential at different solution concentration of [Br-].

Expected Spectrum from *Ab-Initio* Calculations

Three pieces of information are needed for constructing the spectrum from *ab-initio*: binding energy (BE), which determines the center of individual peak; gaussian broadening, which is assumed to be universal for each species as the commonly observed 1.1 eV Full width at half maximum (FWHM); and lastly intensity I, which can be calculated given the parameters (L, λ, C, Θ) defined in the last section. The solution [Br-] ion and surface [Br-] ion intensity can be calculated using the following formulas assuming the exponential decay of signals:

$$I(bulk) = I0 * Cbulk * \int_{h=0}^{h=L} \exp\left(\frac{-h}{\lambda}\right) dh$$

$$I(surface) = I0 * Csurface * \exp\left(\frac{-L}{\lambda}\right) * ¿ \int_{h=0\,Å}^{h=2.6\,Å} \exp\left(\frac{-h}{\lambda}\right) dh ¿$$

The proportionality is defined in I0, which is a function of the cross-section of the element of interest, the incident angle, and an equipment-dependent constant. In the current study the incident angle and equipment are the same, and I0 is the same for surface Br and solution Br. Csurface is in the same unit (mol/m^3) as Csolution. Csurface can be easily converted from Θ (in unit of monolayer) using the area of unit area (2.96 x 2.96 $Å^2$) of Au surface and the average height (2.6 Å) of surface Br, which were obtained from DFT and *ab-initio* MD calculations. Whereas the relative position of the peaks (BE difference) is obtained from the average binding energy (BE) differences between surface [Br-] ion and solution [Br-] ion in the 200 equilibrated *ab-initio* MD frames. We found that the surface [Br-] ion is 0.8 eV higher in binding energy than solution [Br-] ion. The spin-orbit splitting is 2:3 and 1.0 eV apart. Details of the binding energy calculation is described in the methodology section. The constructed spectrum from *ab-initio* is shown in **Figure 4**.

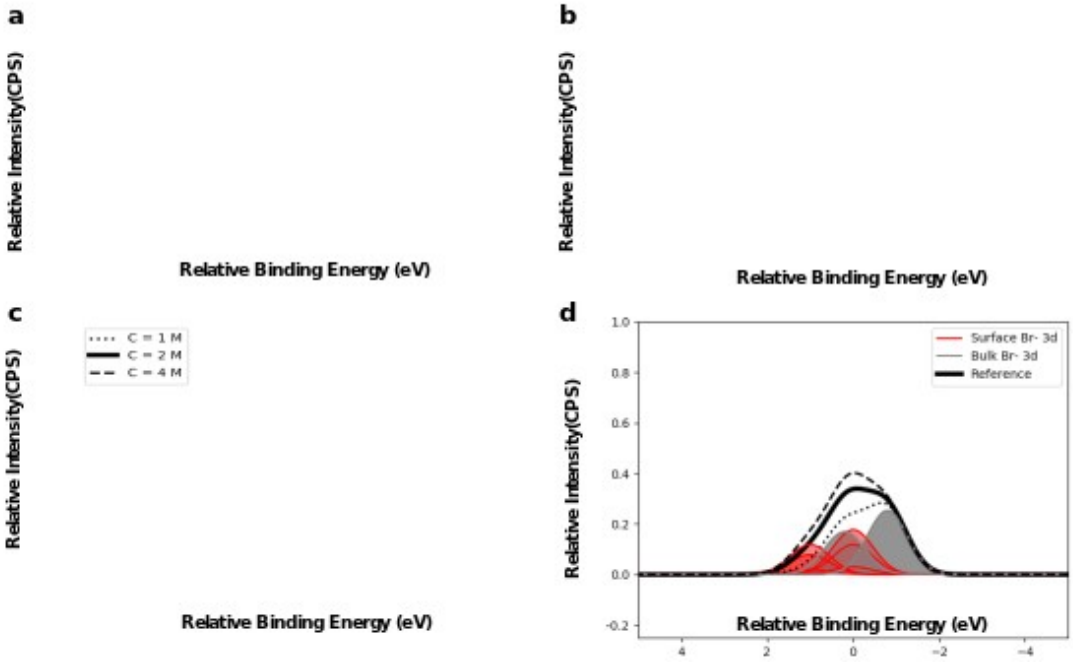

Figure 4. We start with the parameters that generates the spectrum from *ab-initio* (black thick line in **Figure 4**) that best resembles the symmetrical feature, see black thick line of **Figure 1c** and direct comparison in **Figure 6**. We then used these parameters combinations (C =2 M, Θ = 0.4 ML, L = 10 nm, λ = 11 nm) as our basis (black thick line) and show how different the spectroscopic features we expect to see varying individual parameter. The gray areas are the signals from the solution [Br-] ion, and the red areas are the signals from the surface [Br-] ion. The solution [Br-] ion signal and surface [Br-] ion signal together adds to the total intensity (black line). With calculated binding energy BE, intensity, as well as a uniform gaussian broadening, we can create the spectrums from *ab-initio*. **a)** We fix C, Θ, λ and are varying the bulk liquid layer thickness L from 5 nm (left) to 10 nm (middle), and then to 30 nm (right), and we found that the effect of L is shifting the spectrum left and right. **b)** we fix C, Θ, L, and are varying the inelastic mean free path λ from 5 nm (low), to 11 nm (middle), and to 15 nm (high). **c)** We fix Θ, L, λ and vary solution [Br-] ion concentration from 1M (low), to 2M (middle), and to 4 M (high), and the 4 M has same concentration in experimental reference spectrum **Figure 1d**). **d)** We fix C, L, λ and vary surface [Br-] ion coverage from 0.1 ML (low), to 0.4 ML (middle), and to 0.6 ML (high).

Region of Visibility

While the spectroscopic feature from the Br 3d solid/liquid APXPS measurement depends on the 4-dimensional space of bulk solution concentration (C), surface coverage (Θ), bulk liquid layer thickness (L), and inelastic mean free path (λ), it is worthwhile to predict and provide a general guidance of the visibility region for surface [Br-] ion or other solid/liquid systems alike. In **Figure 5**, we investigated the influence of two measurement related parameters (bulk liquid layer thickness (L), and inelastic mean free path (λ)) and plotted the idealized landscape of visibility for such solid/liquid interfacial systems. The visible region (outlined using red dashed line in **Figure 5**) must satisfy the following constraints:

- In order to differentiate surface species from that in bulk solution, the intensity ratio of I (bulk)/I (surface) must be sufficiently small. In this case, we define 10 times as the threshold, as indicated by the dotted red line on the color bar of **Figure 5**. The visible area must be black or gray.
- The experimental evidence of no obvious solution [Br-] ion signal before 0.6 V vs. Ag/AgCl indicates that there is an absolute minimum value for the detection of Br 3d core-level signal, which is estimated to be 2 M and represented as the vertical black line at x = 2 M in **Figure 5**. The visible area must be to the right of the vertical black line. The cross-section for Br 3d core-level is comparatively low, and for other elements and their corresponding core-levels, this vertical line will shift to the left, and resulting in a bigger visible area.
- The adsorption isotherm as discussed in **Figure 4** puts an upper limit on the maximum surface coverage of surface [Br-] ion, which is in the range of 0.4 - 0.5 ML. For simplicity, we represented this limit as a horizontal black line at y = 0.4 ML in **Figure 5**. The visible area must be below the horizontal black line.

To summarize, the visible area is outlined by red dotted triangle in **Figure 5**. For maximum visibility, it is suggested to collect spectrum at a thinner liquid layer thickness, although technically difficult to get the analyzer cone to be too close to the interface, as shown in **Figure 5 a, b, c**. And it is also suggested to collect spectrum at a higher photon energy within the limit of tender X-ray (1 – 5 keV) due to a longer inelastic mean free path, as shown in **Figure 5 d, e, f**. However, if the photon energy increases too much, to the region of hard X-ray, we may suffer from a decrease in cross-section. [37]

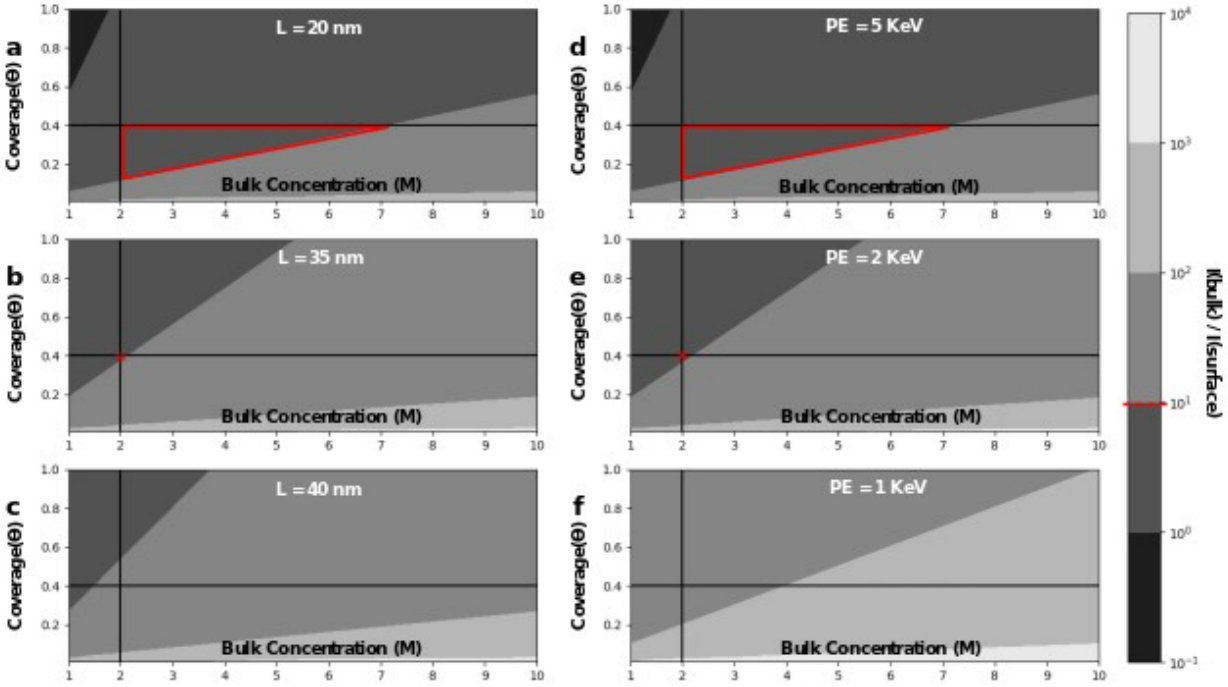

Figure 5. Contour plot shows the region of visibility at various experimentally controllable conditions. No visibility of the surface species if liquid layer thickness is over 35 nm or photon energy is less than 2 keV. **a)** and **d)** Visible area is shown as the red triangular area, which is taken as the intersection of the upper limit of adsorption isothermal (horizontal black line at coverage = 0.4 ML); the lower limit of visibility of Br 3d core-level (vertical black line at bulk concentration = 2 M); and lastly, a high I (bulk) / I (surface) ratio (the black and dark gray region, underneath the red dotted line). **b)** the upper limit of layer thickness is estimated to be around 35 nm at PE = 5 keV, corresponding to λ = 15 nm. **c)** above 35 nm, for example L = 40 nm, there's no intersection satisfying the constraints defined in text, and therefore no visibility for surface [Br-] even if it is presented at the interface. **e)** the lower limit of photon energy is estimated to be around 2 keV, corresponding to λ = 6.5 nm, at the typical layer thickness of 20 nm. **f)** below 2 keV photon energy, there's no visibility of surface [Br-] even if it is presented at the interface.

Motivation for Constructing the Spectrum *Ab-initio*

Generalizing from the present example of Au dissolution with Br- ion, we wish to provide a workflow that allows the construction of solid/liquid APXPS spectrum *ab-initio*. The common practice in the field is usually "fitting experimental spectrum" rather than "constructing spectrum *ab-initio*". However, there is a fundamental difference between "fitting experimental spectrum" and "constructing spectrum *ab-initio*". The former is not generalizable, and it is system specific. A much harder, yet impactful question is how to predict a spectrum given any chemical system and reaction condition, if no experimental spectrum is readily available for fitting. With that said, this later goal of "construct spectrum *ab-initio*" is generalizable to other systems and reaction conditions because the workflow that we described and elaborated (*ab-initio* MD -> DFT -> analytical model -> *ab-initio* constructed spectrum) in the previous sections for constructing spectrum *ab-initio* is universal. First, the *ab-initio* Molecular Dynamics calculation provided the atomic level structures with thermal fluctuations in the equilibrated frames. Second, DFT level calculation on the representative, thermodynamically equilibrated structure (shown in **Figure 1b**) predicts the binding energy (BE) of surface and bulk solution species. Every chemical species' signal is expected to be a gaussian distribution. The binding energy (BE) is the center of the gaussian distribution. The same broadening of 1.1 eV was used to account for thermal fluctuations. Third, the analytical model (with parameter space derived and defined in previous sections) allows us to get the scaling of signal intensity (gaussian area) of each species. Lastly, we arrive at the *ab-initio* constructed spectrum (**Figure 4**), which could then be used to compare with the experimentally observed spectrum.

Scientific advancement in applications such as catalysis, batteries, and energy related materials involve characterization and understanding fundamental atomic level behaviors at the solid/liquid interface. The users of synchrotron-based facilities normally have a material science, synthesis, or engineering background and they rely on the surface-sensitive ambient pressure XPS technique to probe the interface of interest. The calendar for conducting these experiments is very limited (one day a month, or 3-4 consecutive days every 6 months), and normally there's no chance to iteratively perform the experiments with adjusted or updated experimental settings. Despite all the advantages (e.g. improved coherence, better resolution, increased flux, tunable probing depth, ambient pressure, etc.) at synchrotron-based facilities, this working style of synchrotron-based measurement makes prior experimental planning pivotal for success. Experimental planning includes sample preparation, and more importantly, selecting the right parameters (Photon Energy, Probing Liquid Layer Thickness) beforehand, because these parameters are tunable at soft X-ray synchrotron-based facilities, whereas they are not always tunable in lab-based system. As a result, we decided to explicitly depict the role of such experimental parameters, and their relationship with respect to the observed spectrum.

Lastly, we want to make the point that even though the chemistry did not change, the observed spectrum can be different because of different experimental parameters. Unfortunately, the natural and potentially undesirable tendency is to interpolate these differences as a change in chemistry. Showing this procedure of "constructing spectrum *ab-initio*" and encouraging others to go through the same type of procedure (*ab-initio* MD -> DFT -> analytical model -> *ab-initio*

constructed spectrum) for their own system of interest helps address a fundamental challenge to definitively distinguish a new spectroscopic feature that represents truly new chemistry from an artifact of a specific set of experimental parameter choices.

Conclusion

Most of the chemical reactions in catalysis, electrocatalysis, corrosion, and energy storage systems etc. are happening at the solid/gas or solid/liquid interface, and the goal of characterization is naturally differentiating and identifying the surface species and bulk solution species through the distinctive spectroscopic features. However, the setup for solid/liquid Ambient Pressure XPS experiment generally has the surface adsorbed species (~Å scale) buried underneath a bulk electrolyte (~10 nm scale) layer, yielding a weak signal of the target surface adsorbed species. In this example system of Br ion dissolving gold, we demonstrated a procedure of connecting electronic structure information, chemical, and electrochemical information from *ab-initio* calculations (DFT and MD) to experimentally obtained X-ray photoelectron spectrum. This workflow of constructing spectrum *ab-initio* (*ab-initio* MD -> DFT -> analytical model -> *ab-initio* constructed spectrum) is universal and we are merely using Au/Br system as an example. First, the *ab-initio* Molecular Dynamics calculation provided the atomic level structures with thermal fluctuations in the equilibrated frames. We used the average of the last 200 equilibrated frames to extrapolate the structural coordinates for surface species and solution species. Second, we conducted DFT level calculation using the final state approach on the representative, thermodynamically equilibrated structure (shown in Figure 1b) to extrapolate the binding energy (BE) of surface species and species in the bulk solution. The result from DFT is that the binding energy (BE) of these two species are 0.8 eV apart. Every chemical species' signal is expected to be a gaussian distribution, and naturally information needed for construction of this gaussian includes the center, the broadening, and the scaling/area. The binding energy (BE) is the center of the gaussian distribution. The same broadening of 1.1 eV was used to take thermal fluctuations into account. Third, the analytical model (with parameter space derived and defined) allows us to get the scaling of signal intensity (gaussian area) of each species. Lastly, we arrive at the *ab-initio* constructed spectrum (Figure 4).

Walking through this procedure of constructing spectrum *ab-initio* allows us to advance the experimental planning knowledge at synchrotron facilities by illustrating the delicate balance of experimental conditions, including the chemical condition (bulk solution concentration (C), and surface coverage (Θ), as well as measurement condition (bulk liquid layer thickness (L), and inelastic mean free path (λ)) that would lead to the desired spectroscopic features with clear visibility for differentiating surface [Br-] and solution [Br-] ion, and the same framework can be extended to other systems, given the specific parameters of the interested systems.

Acknowledgement

This work was supported by a User Project at The Molecular Foundry and its compute cluster (vulcan), managed by the High Performance Computing Services Group, at Lawrence Berkeley National Laboratory (LBNL), and portions of this work used the computing resources of the

National Energy Research Scientific Computing Center (NERSC), LBNL, both of which are supported by the Office of Science of the U.S. Department of Energy under Contract No. DE-AC02-05CH11231. The Advanced Light Source is supported by the Director, Office of Science, Office of BES, of the US DOE under Contract DE-AC02-05CH11231. J.Q., and E.J.C. were supported by an Early Career Award in the Condensed Phase and Interfacial Molecular Science Program, in the Chemical Sciences Geosciences and Biosciences Division of the Office of Basic Energy Sciences of the U.S. Department of Energy under Contract No. DE-AC02-05CH11231.

Data Availability Statement

The data that support the findings of this study are available from the corresponding author upon reasonable request.

Appendix

Methodology Section

Experimental Method

Beamline 9.3.1 at Advanced Light Source (ALS, Lawrence Berkeley National Laboratory) is equipped with a bending magnet and a Si (111) double crystal monochromator having a total energy range between 2.1 and 6.0 keV ('tender' X-ray range). We followed the same experimental procedure as described in reference [28]. For the electrochemical interface, the electrolyte was comprised of a 1 M KBr + 6 M KF aqueous solution. For the bulk $AuBr_4^-$ solution was from a 1 M Au_2Br_6 aqueous solution.

Adsorption Isotherm of Br^- ions

Following early ideas of Graham [39] and the Parson's analysis of the double layer capacitance [40], the surface coverage of specifically adsorbed species can be estimated using the "Hurwitz-Parsons" method [41]. According to this method, the excess surface concentration Γ_{Br^-} (mol/area) can be obtained from the thermodynamic relationships:

$$\frac{1}{k_B T}\left(\frac{\partial\left(\sigma^0-\sigma\right)}{\partial \ln x}\right)_{\varphi}=-\text{¿¿or}$$

$$\frac{1}{k_B T}\left(\frac{\partial\left(\varphi^0-\varphi\right)}{\partial \ln x}\right)_{\sigma}=\text{¿¿,}$$

where σ^0 or φ^0 are surface charge density or electrode potential of a reference system (no specifically adsorbing ions in the solution of the same ionic strength) and x – is the molar fraction of the specifically adsorbing species (Br^- ions). In practice, Γ_{Br^-} is determined as a slope of the surface tension γ with respect to ln x: $\Gamma_{Br^-}=\frac{1}{k_B T}\left(\frac{\partial \gamma}{\partial \ln x}\right)_{\varphi}$ ¿and γ¿, where $C_{dif}(\varphi; c)$ is the differential capacitance of the double layer at a fixed solution concentration of Br^- ions, and the

integration constants are the potentials of the zero charge (PZC) and a sufficiently negative electrode potential where no adsorbed Br^- ions are expected (a potential at which all differential capacitance curves coincide, e.g. $\varphi = -1.0\,V$ (vs. Ag/AgCl)).

Ab-initio MD Calculation

The input AIMD structure (i.e. set of atomic coordinates) of the equilibrated electrolyte is obtained from classical MD trajectory using the tip3p_charm force field. The slab of the electrolyte was then combined with the slab of gold (111 surfaces, 3 layers) with the top layer pre-optimized. The parameters of the simulation cells are listed in Table S1. Using a sampling of 0.5 fs, we performed AIMD simulations within canonical NVT ensemble at 300 K with the Nose-Hoover thermostat [42] (with characteristic timestep of 100 fs with the Nose-Hoover chain of length 3) and periodic boundary conditions were carried out using Quickstep module of the CP2K package [43]. The total energy was sampled at the Γ-point only. The valence electrons were treated explicitly at the DFT level using the revPBE parametrization functional and a triple-ζ basis set with two additional sets of polarization functions (TZV2PX) [44] and the energy grid cutoff was set as 320 Ry. The core electrons on all atoms were treated using norm-conservative Goedecker-Teter-Hutter (GTH) pseudopotentials [45]. Long-range dispersive forces were treated with DFTD3 empirical Grimme correction [46]. 5 ps equilibration was followed by 25 ps AIMD trajectory.

System	# of molecules in the box	Equilibrated box parameters (A)
~ 6M KBr in water next to Au (111) surface	16K, 16Br, 108Au 119 H_2O	17.63x15.58x28.0

Table S1. Parameters of ab initio MD simulations.

Binding Energy Calculation

Equilibrated frames of *ab-initio* MD trajectory were taken as the structures for binding energy (BE) calculations. The relative XPS core-level shift of surface [Br-] and solution [Br-] are calculated in VASP [47] at PBE-D3 level [48]. There are two approaches for the calculation of relative core-level shift: the initial and final approximation. In the initial state approximation, Kohn-Sham eigenvalues of the core states is subsequent to the self-consistent determination of the charge density associated with the valence electrons. [49] Theoretical studies report that initial approach often reproduces the experimental observations very well for metallic surfaces [50, 51], especially if the adsorbates are far from the metal surfaces, where the relaxation time is longer than near metal core-hole pair. The binding energy of [Br-] ion is calculated to be the same in KBr solution, AuBr3 solution and AuBr solution, which are all possible sources for Solution [Br-] ion.

Figure 6 Comparison of the Experimental and Theoretical Spectrum

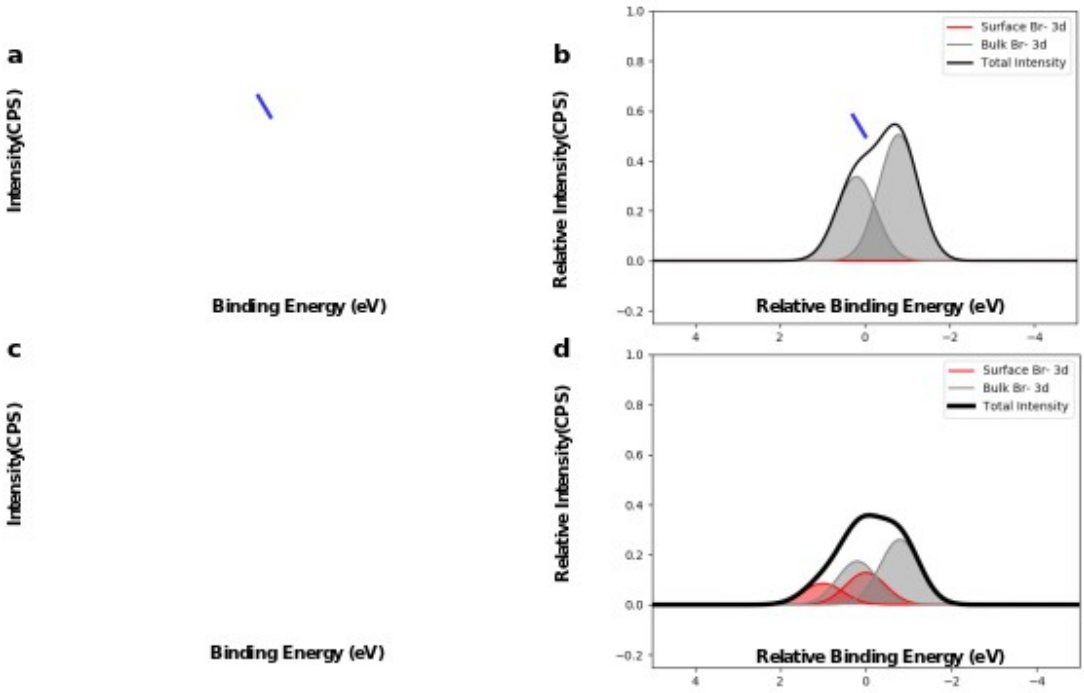

Figure 6 Direct Comparison of the Experimental and Theoretical Spectrum. The blue arrow points out the concave and asymmetrical feature of the reference spectrum, which does not show the signal from surface Br. **a)** Experimental spectrum of 1 M $AuBr_4$- (4 M [Br-]) bulk solution. **b)** Theoretical spectrum of 1M $AuBr_4$- (4M [Br-]) bulk solution, created using parameters C =4 M, Θ = 0.0 ML, L = 10 nm, λ = 11 nm at PE = 4 KeV. **c)** Experimental spectrum of Au dissolved in 1 M KBr solution at 0.6 V vs. Ag/AgCl, the increased Br 3d signal is due to the dissolution of Au and the formation of $AuBr_4$- , therefore increasing the local concentration of solution [Br-] ion to more than 1 M. **d)** Theoretical spectrum derived from *ab-initio* that best resembles the spectrum in **c)**, the parameters used to create this spectrum **d)** are C =2 M, Θ = 0.4 ML, L = 10 nm, λ = 11 nm at PE = 4 KeV.

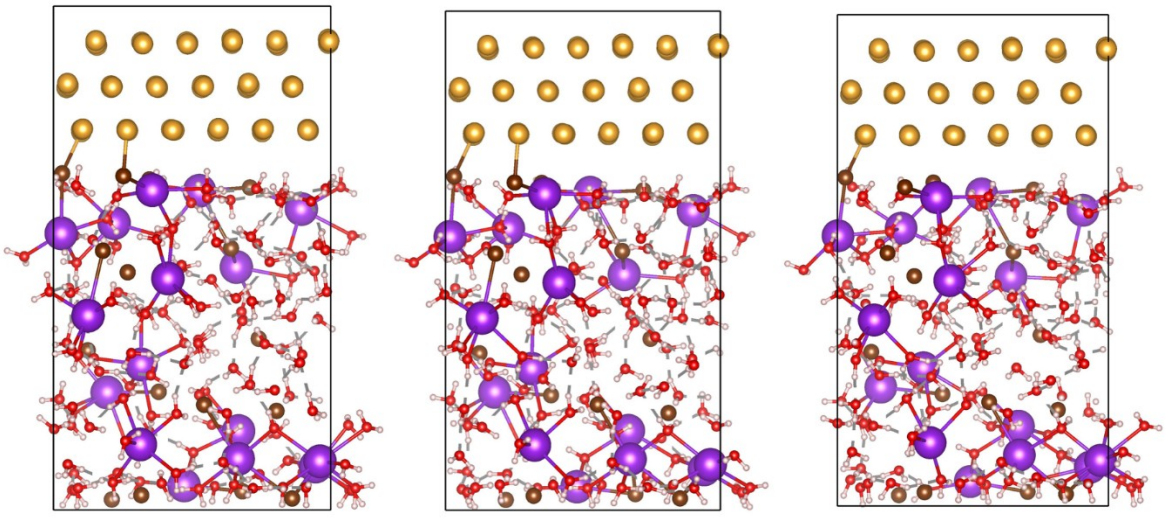

Figure 7 Atomic scale illustrations of the surface species layer and solution species layer, from equilibrated snapshots of *ab-initio* MD calculation. From left to right are snapshot at the last 100, 200, and 400 frames.

References

[1] L. Bocquet, and E. Charlaix, Chemical Society Reviews **39** (2010) 1073.
[2] X. Liu *et al.*, Nat Commun **10** (2019) 32.
[3] S. Nitopi *et al.*, Chem Rev (2019)
[4] E. Boutin *et al.*, Angew Chem Int Ed Engl **58** (2019) 16172.
[5] J. Bao *et al.*, ACS Appl Mater Interfaces **12** (2020) 2243.
[6] K. Chu *et al.*, ACS Appl Mater Interfaces **12** (2020) 7081.
[7] J. Duan *et al.*, Angew Chem Int Ed Engl (2020)
[8] L. He *et al.*, Angew Chem Int Ed Engl **59** (2020) 3544.
[9] K. Lu *et al.*, J Am Chem Soc (2020)
[10] L. Ge *et al.*, J Phys Chem Lett **11** (2020) 869.
[11] S. Haschke *et al.*, Nat Commun **9** (2018) 4565.
[12] Y. Ping, R. J. Nielsen, and W. A. Goddard, 3rd, J Am Chem Soc **139** (2017) 149.
[13] G. Rajeshkhanna *et al.*, ACS Appl Mater Interfaces **10** (2018) 42453.
[14] H. Shin, H. Xiao, and W. A. Goddard, 3rd, J Am Chem Soc **140** (2018) 6745.
[15] H. Xiao, H. Shin, and W. A. Goddard, 3rd, Proc Natl Acad Sci U S A **115** (2018) 5872.
[16] X. Huang *et al.*, Science **348** (2015) 1230.
[17] M. Li *et al.*, Science **354** (2016) 1414.
[18] W. Xu *et al.*, Angew Chem Int Ed Engl **59** (2020) 3511.
[19] C. Liu *et al.*, J Am Chem Soc **141** (2019) 2884.
[20] S. Ganapathy *et al.*, Chemistry **17** (2011) 14811.
[21] D. Molina Piper *et al.*, Nat Commun **6** (2015) 6230.
[22] N. L. Drenchev *et al.*, J Vis Exp (2020)
[23] J. H. Raberg *et al.*, J Phys Chem Lett **10** (2019) 3381.
[24] A. Sayama *et al.*, Phys Chem Chem Phys **22** (2020) 2580.
[25] Y. Zhou *et al.*, Nat Nanotechnol (2020)
[26] D. E. Starr *et al.*, Chem Soc Rev **42** (2013) 5833.
[27] L. Trotochaud *et al.*, J Phys Condens Matter **29** (2017) 053002.
[28] M. Favaro *et al.*, Nat Commun **7** (2016) 12695.
[29] M. Favaro *et al.*, J Am Chem Soc **139** (2017) 8960.
[30] C. H. Wu, R. S. Weatherup, and M. B. Salmeron, Phys Chem Chem Phys **17** (2015) 30229.
[31] Y. H. Lu *et al.*, Nano Lett **19** (2019) 5388.
[32] B. Pesic, and V. C. Storhok, Metallurgical Transactions B **23** (1992) 557.
[33] B. Pesic, and R. H. Sergent, Metallurgical and Materials Transactions B **24** (1993) 419.
[34] M. F. Lichterman *et al.*, Energy & Environmental Science **8** (2015) 2409.
[35] S. Tanuma, C. J. Powell, and D. R. Penn, Surface and interface analysis **35** (2003) 268.
[36] H. Shinotsuka *et al.*, Surf Interface Anal **49** (2017) 238.
[37] S. Axnanda *et al.*, Sci Rep **5** (2015) 9788.
[38] A. Baskin, and D. Prendergast, J Chem Phys **150** (2019) 041725.
[39] D. C. Grahame, and B. A. Soderberg, The Journal of Chemical Physics **22** (1954) 449.

[40] R. Parsons, Transactions of the Faraday Society **55** (1959) 999.
[41] H. D. Hurwitz, Journal of Electroanalytical Chemistry (1959) **10** (1965) 35.
[42] G. J. Martyna, M. L. Klein, and M. Tuckerman, The Journal of chemical physics **97** (1992) 2635.
[43] J. Hutter *et al.*, Rev.: Comput. Mol. Sci **4** (2014) 15.
[44] J. VandeVondele, and J. Hutter, The Journal of chemical physics **127** (2007) 114105.
[45] S. Goedecker, M. Teter, and J. Hutter, Physical Review B **54** (1996) 1703.
[46] S. Grimme *et al.*, The Journal of chemical physics **132** (2010) 154104.
[47] G. Kresse, and J. Furthmüller, Physical review B **54** (1996) 11169.
[48] E. R. Johnson, and A. D. Becke, The Journal of chemical physics **124** (2006) 174104.
[49] L. Köhler, and G. Kresse, Physical Review B **70** (2004) 165405.
[50] Y. Morikawa *et al.*, Surface science **507** (2002) 46.
[51] T. C. Taucher *et al.*, The Journal of Physical Chemistry C **120** (2016) 3428.